Electric resistivity tomography for identification of local anomalies along embankments: 2D or 3D inversion?

Electric resistivity tomography for identification of local anomalies along embankments: 2D or 3D inversion?

F. Pace[1], A. Arato[2], A. Vergnano[3], C. Comina[3], M. Naldi[2], A. Godio[1], L.V. Socco[1,4]

[1] Department of Environment, Land and Infrastructure Engineering (DIATI), Politecnico di Torino, Torino, Italy

[2] Techgea S..r.l., Torino, Italy.

[3] Department of Earth Sciences (DST), Università degli Studi di Torino, Torino, Italy.

[4]Department of Geoscience and Engineering, Delft University of Technology, Delft, The Netherlands.

Introduction.

The geophysical characterization of river embankments is of growing interest in the contest of climate change adaptation actions, aiming at improving the embankment management due to the increased occurrence of floods and extreme events. Electric resistivity tomography (ERT) is one of the geophysical techniques most commonly adopted for the characterization of river embankments because of its high sensitivity to water saturation, infiltration paths and other subsurface discontinuities owed to the electrical resistivity variations (Tresoldi et al., 2019). ERT data are usually acquired along the longitudinal direction of the embankment and then processed following a 2D inversion approach (e.g., Arato et al., 2022). However, the typical embankment geometry, composed of a narrow crest and two lateral slopes laying over a large basis, is strictly 3D and may not be suitable for a 2D interpretation. Previous works have already addressed this issue and introduced some correction factors accounting for the 3D effects (e.g., Hojat et al., 2020). However, little work focused on 3D direct and inverse modelling of ERT data acquired on embankments. This study investigates numerically a 3D characterization of embankments by means of 3D forward and inverse ERT modelling on 3D geometry, in order to demonstrate the potential advantages with respect to 2D inversion.

Method: 2D and 3D inversion of ERT data from embankments.

The ERT forward and inverse modelling was performed in ResIPy, an open-source package that performs 2D and 3D modelling of geoelectrical data (Blanchy et al., 2020; Doyoro et al., 2022; Loke et al., 2013). ResIPy is based on the codes R2, cR2 and R3t, which perform a weighted least-squares inversion of the data with Occam's regularization (Binley and Kemna, 2005). In the present study, the 2D and 3D inversions adopted the regularized inversion with linear filtering and normal regularization, but other inversion settings are available.

We created a 3D model domain to define a model as close as possible to a true embankment geometry, thus including a crest hosting the electrode line, the lateral slopes and the embankment base. ResIPy includes a model generator based on the electrode positions and a mesh generator based on the software Gmsh (Geuzaine and Remacle, 2009; http://gmsh.info). Gmsh is an external tool suitable for the creation of complex meshes and hence the reproduction of a specific embankment geometry. The mesh for 2D inversion was generated with default settings in ResIPy, that calls Gmsh. For 3D modelling, the default mesh generated in ResIPy would not have included the embankment geometry (slopes and crest). Therefore, our 3D mesh was externally created in Gmsh by running a customized python code that accurately reproduced the embankment slopes. This also ensured a fine discretization close to the electrodes and good acceptability of runtime in ResIPy.

A case study of synthetic data: the 3D model and mesh.

A 3D synthetic model simulating an embankment with different anomalies was created, as shown in Fig. 1. The 3D model is 100 m wide (Y direction), 100 m deep (Z direction) and 300 m long (X direction). The model simulates the embankment body on the top with a crest of 6 m, a height of 4 m and a slope ratio of 1:2. The base of the embankment is 22 m large, and it is surrounded by a wide domain to ensure proper boundary conditions for the modelling. The synthetic model was populated with six anomalies with different sizes, shapes, eccentricity to the electrode line and resistivity values (see Fig. 1 for details). These anomalies represent the main features that can be encountered inside an embankment: structural discontinuities, animal burrows, pipelines. The resistivity of the background was set equal to 100 Ωm.

A first set of synthetic data were generated by using two different sequences, one for the dipole-dipole configuration (DD) and another one for the Wenner-Schlumberger configuration (WS). The electrode line was located in the centre of the embankment crest (represented by the Y = 0 axis), was 287 m long and composed of 288 electrodes (1 m of spacing). The simulated acquisition for these synthetic data considered 72 electrodes for the base acquisition and the 9 roll-along acquisitions, each composed of 24 electrodes. The DD sequence had around 29k quadrupoles, while the WS sequence had around 27,2k quadrupoles. The pseudo-sections of apparent resistivity data generated on the 3D synthetic model with 3D forward modelling are depicted in Fig. 2 a) and b) for DD and WS configurations, respectively.

Other synthetic data were generated by shifting the whole electrode line to different positions on the embankment crest. The electrode line was simulated on the Y = 2 and Y = -2 axes of the 3D model (not shown here). The objective of this sensitivity analysis was to inspect the effects of the closeness of the electrodes to the anomalies and to assess any geometric effects due to the short distance of the electrodes from the edge between the crest and slope of the embankment.

The 2D and 3D meshes were unstructured triangular, based on the advanced code Gmsh (Geuzaine and Remacle, 2009). The mesh for 2D inversion was generated in ResIPy and had around 6k nodes. The mesh for 3D forward modelling was externally created in Gmsh and

composed of around 452k nodes. The mesh specifically created for 3D inversion had around 71k nodes, less than the mesh used in the forward simulation.

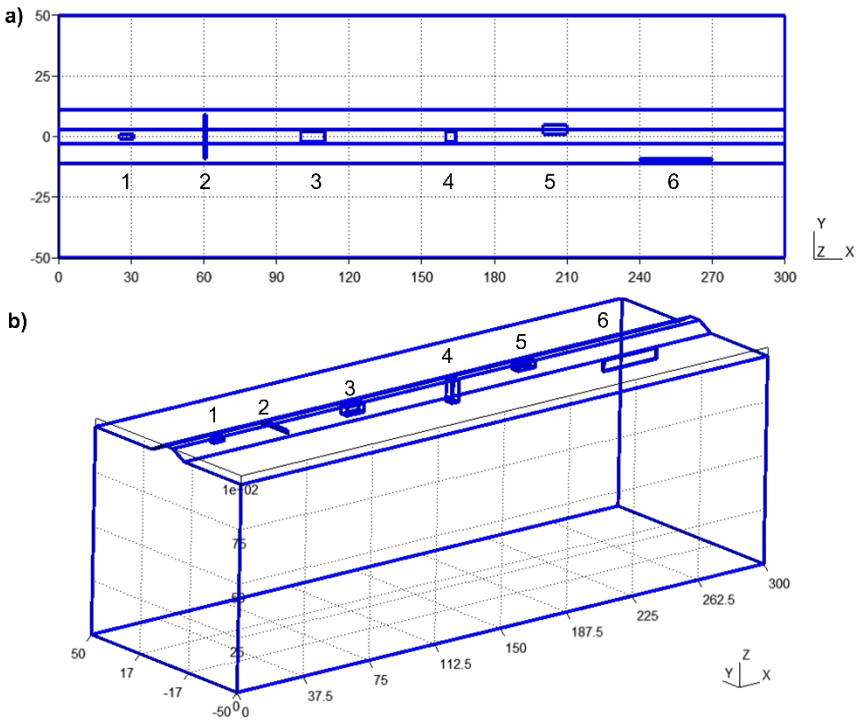

Anomaly n°	Resistivity (Ωm)	Δx, Δy, Δz (m)
1	10	6, 2, 2
2	1000	1, 20, 1
3	10	10, 4, 4
4	10	4, 4, 10
5	10	10, 4, 3
6	1	30, 0.7, 5

Fig. 1 – The 3D model of the embankment containing six different anomalies: a) top view; b) 3D view. The table lists the resistivity value and the dimensions for each anomaly.

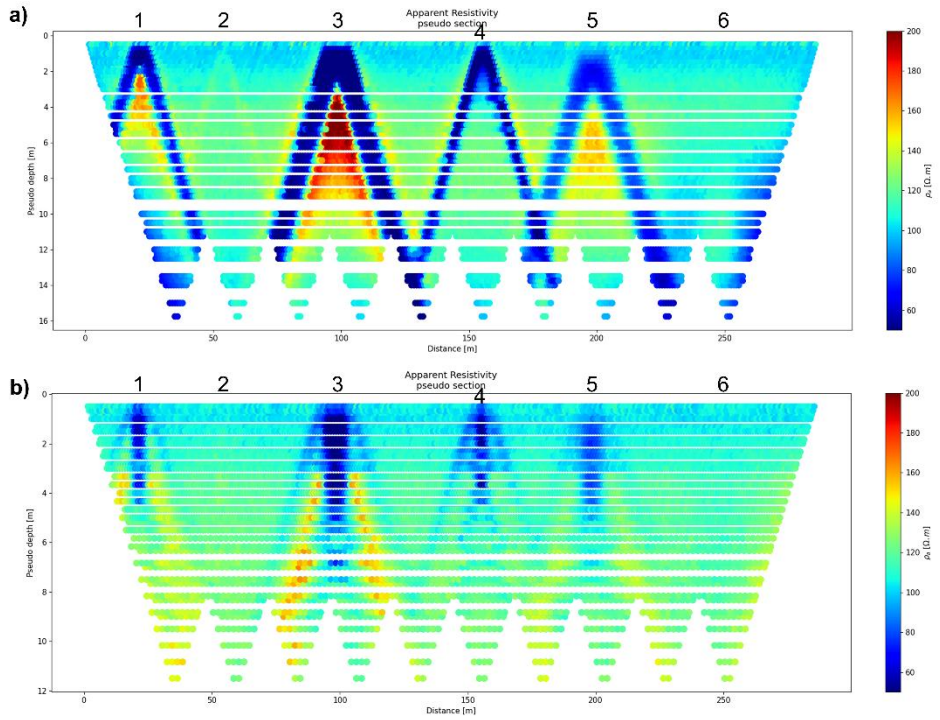

Fig. 2 – The apparent resistivity pseudo-sections from synthetic data after 3D forward modelling in ResIPy: a) dipole-dipole (DD) and b) Wenner-Schlumberger (WS) configurations. The location of the six anomalies is represented.

Results from 2D and 3D ERT inversions.

Both 2D and 3D inversions were initialized by a homogeneous starting model of 100 Ωm, while the a gaussian noise of 2% was added to the synthetic data.

The 2D inversion of DD data ended after one iteration (3 minutes of runtime) and gave a final RMSE = 1.13. The 2D WS inversion ended after one iteration (9 minutes of runtime) and gave a final RMSE = 1.0. A section of the true synthetic model with the six anomalies is represented in Fig. 3 a). The final resistivity models are shown in Fig. 3 b) and c) for DD and WS configurations, respectively.

The 3D inversion of synthetic data was computationally expensive and required around 10 GB of RAM. For DD data, it ended after one iteration (32 minutes of runtime) and gave a final RMSE = 0.61. The 3D WS inversion ran for 5 hours to perform one iteration that gave a final RMSE = 1.17. The vertical slices below the electrode line extracted from the 3D resistivity models are displayed in Fig. 3 d) and e) for DD and WS configurations, respectively.

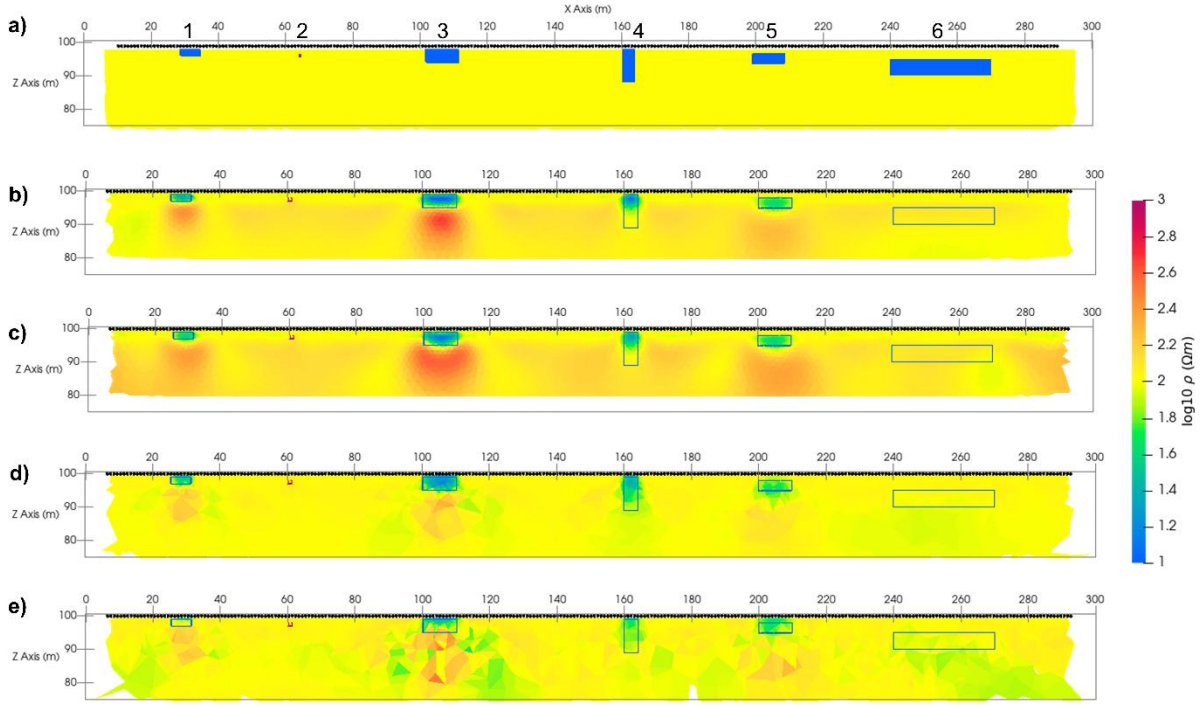

Fig. 3 – a) the section of the 3D synthetic model including all the anomalies (numbered from 1 to 6). The results from b) 2D inversion of DD data, c) 2D inversion of WS data, d) 3D inversion of DD data, e) 3D inversion of WS data.

The models of Fig. 3 b-e) adequately reproduce the anomalies nn. 1, 3, 4, 5, after both 2D and 3D inversions of DD and WS data, while anomalies nn. 2 and 6 were scarcely identified due to their challenging features for ERT modelling in the chosen domain. The main difference between the results of 2D and 3D inversions is that below the conductive bodies n. 1, 3 and 5 there are some resistive artefacts that are stronger in the 2D sections (Fig. 3 b and c) than in the 3D results (Fig. 3 d and e). The shape of the vertical conductor (anomaly n. 4) is better characterized in the 3D model. The background half-space of 100 Ωm is more homogeneous in the 3D sections than in the 2D models, where the background half-space is more resistive than in the 3D sections, maybe due to the geometry of the base of the embankment. The narrow eccentric anomaly n. 6 is scarcely

identified because it is deep and far from the electrodes (Fig. 1). This was expected, but it is worth noting that the 3D inversion models present a resistivity decrease with depth in response of anomaly n. 6 (Fig. 3 d and e). Finally, another advantage of 3D inversion for the embankment geometry is that the lateral extension (in the Y direction) of the subsurface structures can be inspected, thus partially improving the identification of far or eccentric bodies like anomalies nn. 5 and 6.

Conclusion.

We presented a comparison between 2D and 3D ERT inversion of synthetic data generated from a 3D model representing a realistic embankment geometry. The model and mesh generation were specifically carried out in Gmsh, while the ERT forward and inverse modelling was performed in ResIPy. The main outcomes of our study proved that, given an ERT line, the subsurface is better characterized by means of a complete 3D approach especially if the data are acquired over complex or non-flat geometries. Moreover, 3D inversion is more sensitive than 2D inversion to buried anomalies that are deep or eccentric or far from the electrodes thanks to a true characterization of the geometry surrounding the embankment. The ongoing research activity focuses on a field case study that characterizes a real embankment by means of 2D and 3D ERT inversions. New sensitivity analyses on the embankment shape and meshing criteria will be considered, along with further 3D models and meshes.

Acknowledgements.

The research activity of F. P. was carried out within the Ministerial Decree no. 1062/2021 and received funding from the FSE REACT-EU – PON Ricerca e Innovazione 2014–2020. The research activity of A.V., C.C, L.V.S. was carried out within the «GEOCHARME» project – funded by European Union – Next Generation EU within the PRIN 2022 program (D.D. 104 - 02/02/2022 Ministero dell'Università e della Ricerca). This manuscript reflects only the authors' views and opinions and the Ministry cannot be considered responsible for them.

References

Arato A., Vagnon F., and Comina C.; 2022: First application of a new seismo-electric streamer for combined resistivity and seismic measurements along linearly extended earth structures. Near Surface Geophysics, 20(2), 117-134.

Binley A. and Kemna A.: 2005: Electrical Methods, In: Hydrogeophysics by Rubin and Hubbard (Eds.), 129-156, Springer.

Blanchy G., Saneiyan S., Boyd J., McLachlan P., and Binley A.; 2020: ResIPy, an intuitive open source software for complex geoelectrical inversion/modeling, Comput. Geosci., 137, 104423, https://doi.org/10.1016/j.cageo.2020.104423

Doyoro Y. G., Chang P.-Y., Puntu J. M., Lin D.-J., Van Huu T., Rahmalia D. A. and Shie, M.-S.; 2022: A review of open software resources in python for electrical resistivity modelling, Geosci. Lett., 9, 1–16, https://doi.org/10.1186/s40562-022-00214-1

Geuzaine C. and Remacle J.-F.; 2009: Gmsh: A 3-D finite element mesh generator with built-in pre- and post-processing facilities: THE GMSH PAPER, Int. J. Numer. Meth. Eng., 79, 1309–1331, https://doi.org/10.1002/nme.2579

Hojat A., Arosio D., Ivanov V. I., Loke M. H., Longoni L., Papini M., ... and Zanzi L.; 2020: Quantifying seasonal 3D effects for a permanent electrical resistivity tomography monitoring system along the embankment of an irrigation canal. Near Surface Geophysics, 18(Geoelectrical Monitoring), 427-443.

Loke M. H., Chambers J. E., Rucker D. F., Kuras O., and Wilkinson P. B.; 2013: Recent developments in the direct-current geoelectrical imaging method, J. Appl. Geophys., 95, 135–156, https://doi.org/10.1016/j.jappgeo.2013.02.017

Tresoldi G., Arosio D., Hojat A., Longoni L., Papini M. and Zanzi, L.; 2019: Long-term hydrogeophysical monitoring of the internal conditions of river levees. Engineering Geology, 259, 105139.

Corresponding author: francesca.pace@polito.it